A Major Role for a Set of Non-Active Site Mutations in the Development of HIV-1 Protease Drug Resistance†

Salman Muzammil, Patrick Ross, and Ernesto Freire*

Department of Biology and Biocalorimetry Center, The Johns Hopkins University, Baltimore, Maryland 21218

Received October 16, 2002; Revised Manuscript Received November 19, 2002

ABSTRACT: A major problem in the chemotherapy of HIV-1 infection is the appearance of drug resistance. In the case of HIV-1 protease inhibitors, resistance originates from mutations in the protease molecule that lower the affinity of inhibitors while still maintaining a viable enzymatic profile. Drug resistance mutations can be classified as active site or non-active site mutations depending on their location within the protease molecule. Active site mutations directly affect drug/target interactions, and their action can be readily understood in structural terms. Non-active site mutations influence binding from distal locations, and their mechanism of action is not immediately apparent. In this paper, we have characterized a mutant form of the HIV-1 protease, ANAM-11, identified in clinical isolates from HIV-1 infected patients treated with protease inhibitors. This mutant protease contains 11 mutations, 10 of which are located outside the active site (L10I/M36I/S37D/M46I/R57K/L63P/A71V/G73S/L90M/I93L) and 1 within the active site (I84V). ANAM-11 lowers the binding affinity of indinavir, nelfinavir, saquinavir, and ritonavir by factors of 4000, 3300, 5800, and 80000, respectively. Surprisingly, most of the loss in inhibitor affinity is due to the non-active site mutations as demonstrated by additional experiments performed with a protease containing only the 10 non-active site mutations (NAM-10) and another containing only the active site mutation (A-1). Kinetic analysis with two different substrates yielded comparable catalytic efficiencies for A-1, ANAM-11, NAM-10, and the wild-type protease. These studies demonstrate that non-active site mutations can be the primary source of resistance and that their role is not necessarily limited to compensate deleterious effects of active site mutations. Analysis of the structural stability of the proteases by differential scanning calorimetry reveals that ANAM-11 and NAM-10 are structurally more stable than the wild-type protease while A-1 is less stable. Together, the binding and structural thermodynamic results suggest that the non-active site mutants affect inhibitor binding by altering the geometry of the binding site cavity through the accumulation of mutations within the core of the protease molecule.

Drug resistance to HIV-1[1] protease inhibitors usually begins with the appearance of amino acid mutations within the binding site cavity of the enzyme (*1*). Non-active site mutations occur later and have been assigned mostly compensatory functions aimed at neutralizing the detrimental effects of primary mutations on enzyme activity (*2*−*5*). Because active site mutations directly affect the drug/target interface, their mode of action has been interpreted in terms of lost interactions or steric effects created by altered site geometries (*6*−*8*). For example, some active site mutations are known to preferentially affect some inhibitors. Notoriously, I50V affects amprenavir (*9*, *10*), V82F affects ritonavir (*11*), D30N affects nelfinavir (*12*, *13*), and G48V affects saquinavir (*14*). The role of non-active site mutations in inhibitor binding has remained largely elusive, and surprisingly, only a few studies have reported the effects of these mutations on inhibitor binding even though a major role in lowering inhibitor potency was reported (*15*, *16*). The importance of non-active site mutations in drug resistance is emphasized by the observation that strains of HIV-1 that exhibit phenotypic and genotypic resistance to multiple drugs have a constellation of non-active site mutations (3−13) and only one or two active site mutations (*17*, *18*).

Using kinetic analysis and microcalorimetric techniques, we have characterized a resistant mutant form of the HIV-1 protease first identified in clinical isolates of patients treated with protease inhibitors (*15*, *19*). This resistant mutant, ANAM-11, differs from the wild-type protease at 11 positions. Ten of those positions are outside the binding site (L10I/M36I/S37D/M46I/R57K/L63P/A71V/G73S/L90M/I93L) and one (I84V) is inside the binding site cavity. The non-active site mutations are grouped in three regions within the protease molecule. M36I/S37D/M46I/R57K are located in the flap region, M46I being the closest to the binding cavity although its side chain faces outward, L63P/A71V/G73S are located in the β-sheet core, and L10I/L90M/I93L are located in the terminal region close to the dimerization interface of the protease (Figure 1). Olsen et al. (*15*)

† Supported by National Institutes of Health Grant GM 57144. S.M. is a recipient of a fellowship from the American Foundation for AIDS Research (AmfAR 70545−30-RF).

* To whom correspondence should be addressed. Phone: (410) 516-7743. Fax: (410) 516-6469. E-mail: ef@jhu.edu.

[1] Abbreviations: HIV-1, human immunodeficiency virus type 1; A-1, HIV-1 protease active site mutant I84V; ANAM-11, drug-resistant mutant L10I/M36I/S37D/M46I/R57K/L63P/A71V/G73S/I84V/L90M/I93L; NAM-10, HIV-1 protease non-active site mutant L10I/M36I/S37D/M46I/R57K/L63P/A71V/G73S/L90M/I93L; ITC, isothermal titration calorimetry; DSC, differential scannning calorimetry.

10.1021/bi027019u CCC: $25.00
Published on Web 01/01/2003

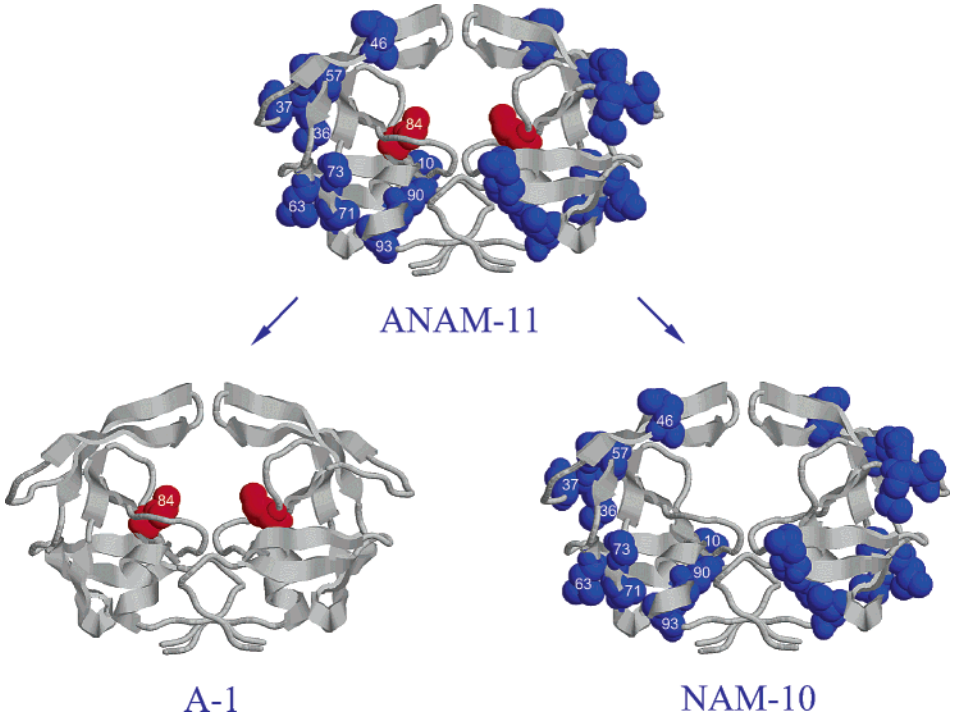

FIGURE 1: Structure of HIV-1 protease showing the mutations used in this study. The residue in red represents the location of the active site mutation I84V, and the residues in blue represent the position of the non-active site mutations, L10I/M36I/S37D/M46I/R57K/L63P/A71V/G73S/L90M/I93L.

performed kinetic analysis on a protease carrying the same set of active and non-active site mutations and concluded that the non-active site mutations played a major role in engendering resistance. To understand the role of active site and non-active site mutations, we performed precise binding studies on ANAM-11 and two additional HIV-1 protease mutants, one containing only the active site mutation (A-1) and the other containing only the non-active site mutations (NAM-10). The enzymatic characteristics and the binding energetics of the association between ANAM-11, A-1, and NAM-10 with four protease inhibitors currently in clinical use (indinavir, nelfinavir, saquinavir, and ritonavir) were studied by fluorescence inhibition assays and high-sensitivity isothermal titration calorimetry, respectively. The results of these studies indicate that the non-active site mutations in ANAM-11 are responsible for most of the observed loses in inhibitor binding affinity. Furthermore, these studies suggest that non-active site mutations not only compensate deleterious effects triggered by the initial active site mutations but are also responsible for very large drops in inhibitor binding affinity as drug-resistant strains of the virus become established.

EXPERIMENTAL PROCEDURES

Protease Mutants. HIV-1 protease containing the mutations L10I/M36I/S37D/M46I/R57K/L63P/A71V/G73S/I84V/L90M/I93L for ANAM-11, L10I/M36I/S37D/M46I/R57K/L63P/A71V/G73S/L90M/I93L for NAM-10, and I84V for A-1 were generated from the B subtype protease as described before (*20*, *21*) by PCR mutagenesis. The gene encoding the B subtype HIV-1 protease was transferred to the pET24 vector (Novagen), where the expression is under control of the T7 promoter. Mutations at selected positions were introduced by using an in vitro site-directed mutagenesis kit (Stratagene), and mutations were confirmed by DNA sequencing. Proteases were expressed in BL21(DE3) cells by adding isopropyl β-D-thiogalactoside (IPTG) to 1 mM once culture density (as determined by absorbance at 600 nm) was 1.5 or greater. All of the protease constructs in this study are on the wild type containing the single Q7K mutation to prevent autocatalysis during the course of microcalorimetric experiments. This protein has enzymatic properties similar to that of the wild-type protease (*22*).

Protease Purification. Protease purification was performed as described before (*23*, *24*) with minor modifications. Plasmid-encoded mutant protease was expressed as inclusion bodies in BL21(DE3) cells. Cells were suspended in extraction buffer (20 mM Tris, 1 mM EDTA, 10 mM 2-ME, pH 7.5) and broken with two passes through a French pressure cell ($\geq$16000 psi). Cell debris and protease-containing inclusion bodies were collected by centrifugation (20000*g* for 20 min at 4 °C). Inclusion bodies were subjected to a sequence of four steps, each one consisting of resuspension (glass homogenizer, sonication) and centrifugation (20000*g* for 20 min at 4 °C). In each step, a different washing buffer was employed: buffer 1 (25 mM Tris, 2.5 mM EDTA, 0.5 M NaCl, 1 mM Gly-Gly, 50 mM 2-ME, pH 7.0), buffer 2 (25 mM Tris, 2.5 mM EDTA, 0.5 M NaCl, 1 mM Gly-Gly, 50 mM 2-ME, 1 M urea, pH 7.0), buffer 3 (25 mM Tris, 1 mM EDTA, 1 mM Gly-Gly, 50 mM 2-ME, pH 7.0), and buffer 4 (25 mM Tris, 1 mM EDTA, 1 mM Gly-Gly, 50 mM 2-ME, 9 M urea, pH 8.0). After the last centrifugation (at 25 °C), protease was recovered in the supernatant. The supernatant obtained was applied to an anion-exchange Q-Sepharose column (Q-Sepharose HP, Pharmacia) previously equilibrated with buffer 4. The protease solution that eluted from the column was pooled and was immediately acidified by addition of formic acid to 25 mM concentration. Precipitation of a significant amount of contaminants occurred upon acidification. Protease at a concentration of 0.1−

0.2 mg/mL was folded by dialysis against 4 L of 30 mM formic acid, pH 2.8, for 4 h. Following dialysis, the pH of protease solution was raised to ~3.8 at 0 °C and then was allowed to increase the temperature to ~25 °C. Sodium acetate buffer, pH 5.5, was added to the protein solution to raise the pH to ~5.0, and the solution was concentrated (~10 mg/mL). Folded protease was desalted into 1 mM sodium acetate and 2 mM NaCl at pH 5.0 using a buffer exchange column (PD-10, Pharmacia) and stored at either 4 or −20 °C (>2.5 mg/mL). After folding, the purity was determined by SDS−PAGE (≥99%).

Inhibitors. Clinical protease inhibitors (indinavir, saquinavir, ritonavir, and nelfinavir) were purified from commercial capsules by HPLC (Waters) as described before (*23*, *24*). Purified inhibitors were lyophilized and stored at −20 °C in the crystalline form (indinavir, nelfinavir) or as suspensions in DMSO (saquinavir, ritonavir). Acetylpepstatin was purchased from Bachem AG and used without further purification.

Enzymatic Assays. The specific activity of the HIV-1 protease preparations was measured by following the hydrolysis of the chromogenic substrate Lys-Ala-Arg-Val-Nle-nPhe-Glu-Ala-Nle-NH_2 (California Peptide Research Inc., Napa, CA), where Nle stands for norleucine and nPhe stands for *p*-nitrophenylalanine as described before (*24*). Briefly, protease was added to a 120 mL microcuvette containing substrate at 25 °C. Final concentrations in the standard assay were 15−30 nM protease, 0−100 mM substrate, 10 mM sodium acetate, and 1 M NaCl at a pH of 5.0. The absorbance was monitored at 300 nm using a Cary 100 UV/visible spectrophotometer (Varian Inc., Palo Alto, CA). An extinction coefficient for the difference in absorbance upon hydrolysis (1800 M^{-1} cm^{-1} at 300 nm) was used to convert absorbance change to reaction rates. Hydrolysis rates were obtained from the initial portion of the data, where at least 80% of the substrate remained unhydrolyzed. Typical wild-type protease preparations hydrolyzed chromogenic substrate at 5−6 s^{-1} (per dimer) at 25 °C.

Alternatively, protease activity was determined by following the increase in fluorescence with hydrolysis of the fluorogenic substrate Arg-Glu(EDANS)-Ser-Gln-Asn-Tyr-Pro-Ile-Val-Gln-Lys(DABCYL)-Arg (Molecular Probes, Eugene, OR). Final concentrations in the standard assay were 15−60 nM protease, 0−100 mM substrate, and 10 mM sodium acetate, pH 5.0. Fluorescence was measured on a CytoFluor fluorescence multiwell plate reader (Applied Biosystems, Foster City, CA) with an excitation wavelength of 360 nm and an emission wavelength of 508 nm. Hydrolysis rates were obtained from the initial portion of the data, where at least 80% of the substrate remained unhydrolyzed.

Isothermal Titration Calorimetry. Isothermal titration calorimetry experiments were carried out using a high-precision VP-ITC titration calorimeter (Microcal Inc., Northampton, MA). The enzyme solution in the calorimetric cell was titrated with inhibitor solutions dissolved in the same buffer (10 mM sodium acetate, pH 5.0, 2% DMSO). The inhibitor concentrations in the experiments were 100−300 μM in the injection syringe. The heat evolved after each injection was obtained from the integral of the calorimetric signal. The heat due to the binding reaction between the inhibitor and the enzyme was obtained as the difference between the heat of reaction and the corresponding heat of dilution. Data were analyzed using Origin 5.0 (Microcal Software Inc., Northampton, MA). In displacement titration experiments, inhibitors were injected into the calorimetric cell containing the protein prebound to a weak inhibitor (acetylpepstatin) as described earlier (*6*). The concentration of acetylpepstatin in the titration cell was in the range of 6−200 μM.

Differential Scanning Calorimetry. The heat capacity function of different HIV-1 protease mutants was measured as a function of temperature with a high-precision differential scanning VP-DSC microcalorimeter (Microcal Inc., Northampton, MA). Protein samples and reference solutions were degassed and carefully loaded into the cells to avoid bubble formation. Exhaustive cleaning of the cells was undertaken before each experiment. Protease samples for thermal stability studies were prepared in 10 mM formate buffer, pH 3.4. Solutions containing 10−60 μM (dimer) protease were scanned at a rate of 1 °C/min from 10 to 85 °C. Reversibility for a single cycle was at least 80%. Data were analyzed by software developed in this laboratory.

RESULTS AND DISCUSSION

Catalytic Activity. The two substrates used in the enzymatic assays, Lys-Ala-Arg-Val-Nle-nPhe-Glu-Ala-Nle-NH2 and Arg-Glu(EDANS)-Ser-Gln-Asn-Tyr-Pro-Ile-Val-Gln-Lys(DABCYL)-Arg, mimic two cleavage sites, KARVL/AEAM, between the capsid protein and nucleocapsid (CA-NCa), and SQNY/PIVQ, between the matrix and capsid proteins in the *Gag* polyprotein precursor. These are two of the most conserved protease cleavage sites in the *Gag* polyprotein, even among different viral subtypes (*25*). The kinetic parameters determined for the HIV-1 mutant proteases and the wild-type protease are summarized in Table 1. Measurements were performed in the presence of 1 M NaCl with both substrates. In addition, for the fluorescence substrate, kinetic experiments were also performed in the absence of NaCl, conditions under which the catalytic efficiency of the protease is known to be very low (*26*). Due to the concentration requirements, only the fluorescent but not the chromogenic substrate could be used in the absence of salt. These experiments demonstrate that, for all situations studied, the catalytic efficiency of the various protease mutants never differs by more than a factor of 4 from the wild-type protease. Similar catalytic efficiencies were reported by Ridky et al. (*27*) for the active site I84V protease mutant. Variations in catalytic efficiencies are even lower if A-1 is compared with ANAM-11. In this case, catalytic efficiencies do not differ by more than a factor of 1.7. These results strongly suggest that, with this particular set of mutations, the role of the non-active site mutations is not to compensate a loss in catalytic efficiency brought about by the active site mutation.

Enzyme Inhibition. The inhibition constants (K_i) of four protease inhibitors in clinical use (indinavir, nelfinavir, saquinavir, and ritonavir) for the wild-type protease and the mutant proteases ANAM-11, A-1, and NAM-10 were determined by using enzyme kinetic assays with the fluorescence substrate [Arg-Glu(EDANS)-Ser-Gln-Asn-Tyr-Pro-Ile-Val-Gln-Lys(DABCYL)-Arg]. Table 2 summarizes the K_i values for all of the inhibitors studied. For the wild-type

Table 1: Kinetic Parameters for Wild-Type and Mutant HIV-1 Proteases

substrate[a,b]	protease type	k_{cat} (s^{-1})	K_M (μM)	k_{cat}/K_M (s^{-1} μM^{-1})
I (KARVL/AEAM)	wild type	10.81 ± 0.26	12.91 ± 0.93	0.84 ± 0.08
(1.0 M NaCl)	ANAM-11	40.8 ± 1.91	27.73 ± 3.26	1.47 ± 0.24
	A-1	44.26 ± 0.77	17.80 ± 0.88	2.48 ± 0.17
	NAM-10	17.59 ± 1.06	18.33 ± 3.05	0.96 ± 0.22
II (SQNY/PIVQ)	wild type	9.31 ± 0.40	9.76 ± 1.00	0.95 ± 0.14
(1.0 M NaCl)	ANAM-11	1.74 ± 0.08	6.95 ± 0.82	0.25 ± 0.04
	A-1	2.43 ± 0.15	5.77 ± 1.05	0.42 ± 0.10
	NAM-10	6.15 ± 0.29	6.26 ± 0.85	0.98 ± 0.18
II (SQNY/PIVQ)	wild type	1.06 ± 0.08	30.54 ± 4.95	0.035 ± 0.008
(0.0 M NaCl)	ANAM-11	1.51 ± 0.06	23.29 ± 2.35	0.065 ± 0.009
	A-1	1.31 ± 0.04	24.65 ± 1.93	0.053 ± 0.006
	NAM-10	1.95 ± 0.05	21.85 ± 1.47	0.089 ± 0.008

[a] All of the experiments were carried out in 10 mM sodium acetate buffer, pH 5.0 at 25 °C, in either the presence or absence of 1 M NaCl. [b] Substrate I is Lys-Ala-Arg-Val-Nle-nPhe-Gln-Ala-Nle-NH_2 and corresponds to the KARVL/AEAM sequence between the capsid and nucleocapsid. Substrate II is Arg-Glu(EDANS)-Ser-Gln-Asn-Tyr-Pro-Ile-Val-Gln-Lys(DABCYL)-Arg and corresponds to the SQNY/PIVQ sequence between the matrix and capsid.

Table 2: Inhibition Constants (K_i) for Wild-Type and Mutant HIV-1 Proteases[a]

inhibitor	wild type (nM)	ANAM-11 (nM)	A-1 (nM)	NAM-10 (nM)
indinavir	0.543 ± 0.057 (1)	1102 ± 51 (2030)	4.4 ± 0.3 (8)	481 ± 54 (890)
nelfinavir	0.254 ± 0.046 (1)	722 ± 75 (2840)	1.9 ± 0.2 (7)	445 ± 50 (1750)
saquinavir	0.463 ± 0.026 (1)	1948 ± 198 (4200)	2.0 ± 0.6 (4)	755 ± 41 (1630)
ritonavir	0.027 ± 0.002 (1)	2107 ± 123 (78000)	0.91 ± 0.33 (33)	340 ± 26 (12600)

[a] The inhibition constants (K_i) were obtained at 25 °C by measuring the change in fluorescence associated with the cleavage of the fluorogenic substrate, Arg-Glu(EDANS)-Ser-Gln-Asn-Tyr-Pro-Ile-Val-Gln-Lys(DABCYL)-Arg, using 5−40 nM protease in 10 mM sodium acetate buffer, pH 5.0, 40 μM substrate, and increasing amounts of inhibitor. The K_i ratios ($K_{i,mutant}/K_{i,WT}$) for the mutant proteases are shown in parentheses.

protease the K_i values are in the subnanomolar range, in agreement with previous studies (*6*, *28*). Against ANAM-11 the inhibition constants for all inhibitors were dramatically weaker and characterized by K_i ratios ranging from 2000 to 78000. The K_i ratios for the protease containing only the single active site mutation (A-1) ranged between 4 and 33, suggesting that most of the observed effect in ANAM-11 was due to the non-active site mutations. In fact, the K_i ratios for the protease containing only the non-active site mutations (NAM-10) ranged between 900 and 12000. These experiments indicate that the set of non-active site mutations is responsible for most of the loss of inhibitory potency, in agreement with the results of Olsen et al. (*15*).

Thermodynamic Dissection of Inhibitor Binding. Calorimetric displacement titration experiments (*6*) were carried out to determine the binding energetics of inhibitors to the mutant proteases. Figure 2 shows the calorimetric displacement titration for saquinavir into the mutant proteases, ANAM-11, A-1, and NAM-10. The left panels show the titration of protease with acetylpepstatin, the low-affinity inhibitor used in the displacement experiments, and the right panels the titration of saquinavir into the HIV-1 mutant proteases prebound to acetylpepstatin. The left panel experiments were used to determine the binding affinities and binding enthalpies of acetylpepstatin to each of the mutant proteases. The dissociation constants, K_d, were determined to be 1140, 328, and 242 nM and the binding enthalpies 5.0, 8.0, and 4.6 kcal/mol for ANAM-11, A-1, and NAM-10, respectively. Similar experiments were performed with the remaining three inhibitors, and the results were analyzed as described before (*6*, *29*). The resulting thermodynamic parameters for all inhibitors are summarized in Table 3. The K_d's measured for indinavir, nelfinavir, saquinavir, and ritonavir agree well with the inhibition constants, K_i, measured in the enzyme inhibition experiments (see Tables 2 and 3). These results also indicate that the main determinant for the loss of inhibitor binding affinity is the set of non-active site mutations. When the different contributions to the Gibbs energy of binding are considered, it becomes apparent that indinavir, nelfinavir, saquinavir, and, to a lesser extent, ritonavir lose significant enthalpic interactions when compared to the wild-type protease. The change in entropic contributions to the binding energy is generally smaller and of opposite sign for A-1. Against the active site mutation the loss in binding enthalpy is partially compensated by an actual gain in binding entropy by all inhibitors. Against the non-active site mutations only saquinavir is able to partially compensate the enthalpic losses with an entropic gain. Ritonavir, on the other hand, loses significantly more entropic than enthalpic contributions to the binding energy, resulting in an overall higher loss in binding affinity against ANAM-11.

The results presented above demonstrate that the set of non-active site mutations in ANAM-11 is the major factor responsible for drug resistance. These mutations bring the binding constant for all inhibitors in clinical use to the micromolar range, effectively rendering them useless in arresting the spread of the virus. Since non-active site mutations do not affect directly inhibitor−target interactions, their mechanism of action involves long-range interactions that propagate to the active site. Two different, not mutually exclusive mechanisms are possible: (1) geometric distortions in the active site due to the cumulative effects of mutations within the structural core of the protease and (2) an increase in the Gibbs energy associated with the conformational change coupled to inhibitor binding.

Structural Stability of the Mutant Proteases. The effects of the mutations on the conformational stability of the

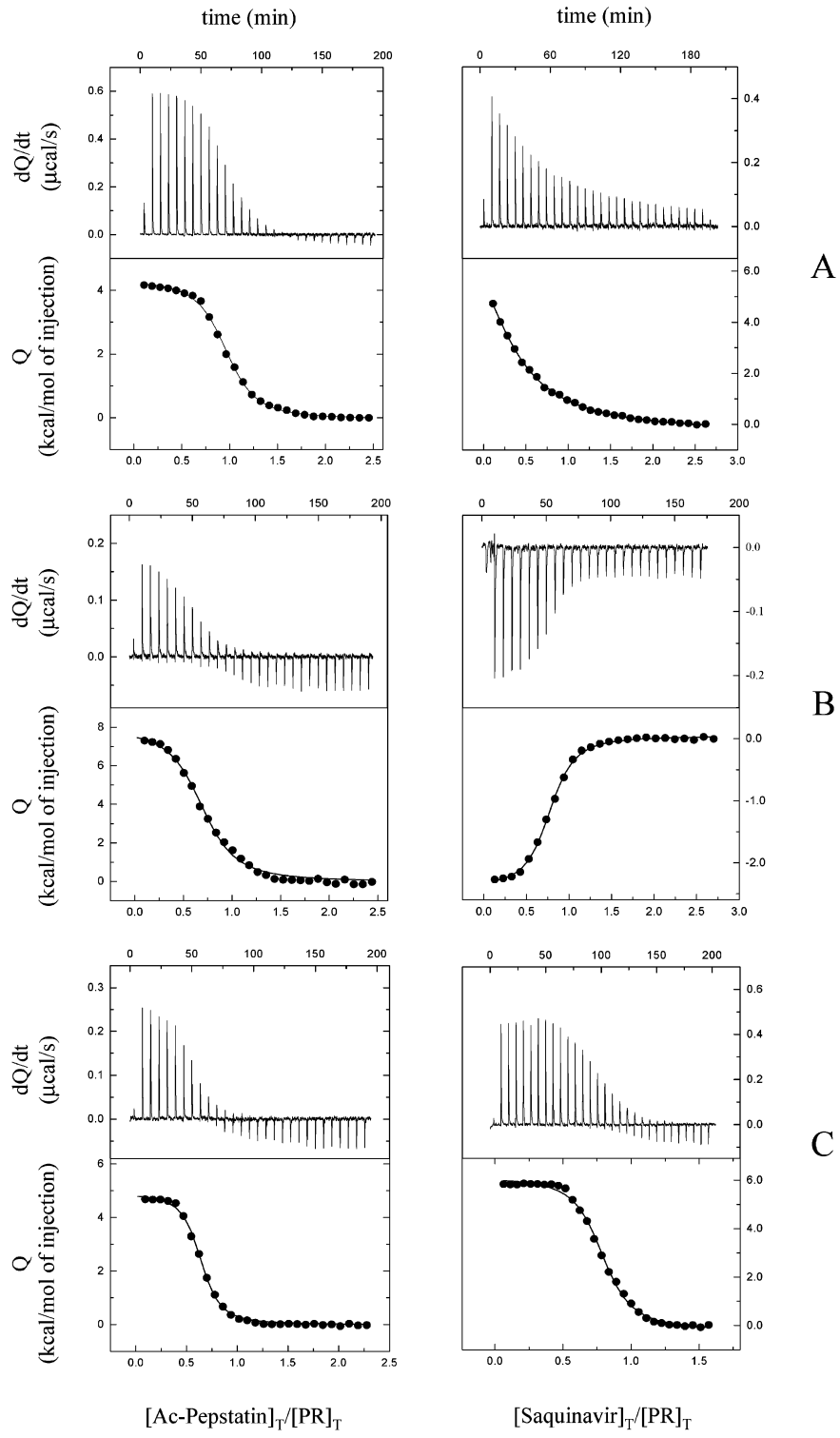

FIGURE 2: Typical set of ITC displacement experiments. The left panels represent the calorimetric titrations of acetylpepstatin into HIV-1 protease mutants ANAM-11 (A), A-1 (B), and NAM-10 (C) and the right panels the titrations of saquinavir into a solution of the corresponding mutant proteases prebound to acetylpepstatin. The experiments were performed in 10 mM sodium acetate buffer, pH 5.0, and 2% DMSO. The data were analyzed as explained before (*6*).

protease in the absence of inhibitors can be evaluated by differential scanning calorimetry. Changes in the structural stability of the unligated protease will influence the binding energetics by altering the energy barrier associated with the obligatory conformational change coupled to inhibitor binding. Figure 3A shows the excess heat capacity function of the wild-type protease, ANAM-11, A-1, and NAM-10 measured by high-sensitivity differential scanning calorimetry. These experiments were performed under similar solvent and protein concentration conditions and indicate that the non-active site mutations increase while the active site mutation decreases the structural stability of the protease. Since the stability of the HIV-1 protease is concentration dependent due to its dimeric nature (*20*), a quantitative analysis of the effects of the different mutations was performed by measuring the concentration dependence of

Table 3: Thermodynamic Parameters for Inhibitor Binding to HIV-1 Proteases

		wild type[a]	ANAM-11	A-1	NAM-10
K_d (nM)	indinavir	0.48 ± 0.01	1900 ± 248	1.8 ± 0.16	538 ± 58
	nelfinavir	0.26 ± 0.005	854 ± 86	0.9 ± 0.17	521 ± 77
	saquinavir	0.40 ± 0.01	2330 ± 264	1.6 ± 0.34	421 ± 49
	ritonavir	0.03 ± 0.001	2270 ± 247	1.6 ± 0.09	375 ± 10
ΔG (cal/mol)	indinavir	−12700	−7800	−11900	−8550
	nelfinavir	−13100	−8300	−12300	−8600
	saquinavir	−12800	−7680	−12000	−8700
	ritonavir	−14400	−7700	−12000	−8800
ΔH (cal/mol)	indinavir	2100	5600	3600	6160
	nelfinavir	2600	3800	4800	5600
	saquinavir	1900	9600	6000	6400
	ritonavir	−3700	−6300	20	−2300
$-T\Delta S$ (cal/mol)	indinavir	−14800	−13400	−15500	−14710
	nelfinavir	−15700	−12100	−17100	−14200
	saquinavir	−14700	−17280	−18000	−15100
	ritonavir	−10700	−1400	−12020	−6500

[a] Adapted from ref *6*. Experiments were performed in 10 mM sodium acetate buffer, pH 5.0, and 2% DMSO at 25 °C.

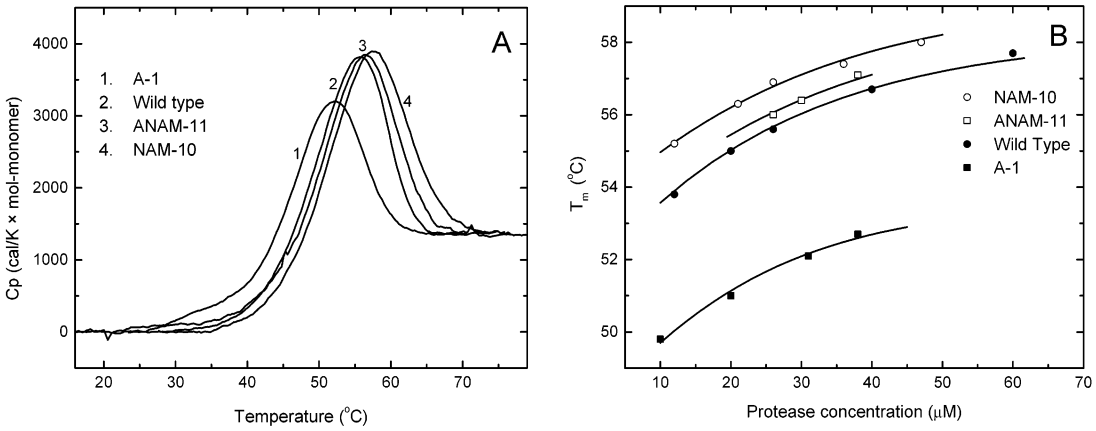

FIGURE 3: (A) Structural stability of the wild-type, ANAM-11, A-1, and NAM-10 HIV-1 proteases as determined by high-sensitivity differential scanning calorimetry (DSC). The experiments were performed in 10 mM sodium formate buffer, pH 3.4. The NAM-10 protease was found to be most stable followed by ANAM-11, wild-type, and A-1 proteases. (B) Concentration dependence of the maximum in the heat capacity function. DSC scans were performed using varying concentrations of protease. The temperature of the maximum in the heat capacity curve is plotted versus protease concentration. The solid continuous lines represent the expected concentration dependence of T_m calculated according to the equation for the stability of a dimeric protein as described in the text.

the stability of all mutants. Previously (*20*), we demonstrated that the thermodynamic stability of the protease molecule can be accounted for by a model in which the dimeric native structure is in equilibrium with unfolded monomers with no detectable dimeric or monomeric intermediates:

$$N_2 \overset{K}{\rightleftharpoons} 2U \tag{1}$$

According to this model, the fraction of molecules that are in the unfolded state, F_u, is given by the equation (*30*, *31*):

$$F_u = \frac{A[(A^2+4)^{1/2} - A]}{2} \tag{2}$$

where A is a function of the equilibrium constant K and the protease concentration:

$$A = \left[\frac{K}{2[\mathrm{HIV}]}\right]^{1/2} = \left[\frac{e^{-\Delta G/RT}}{2[\mathrm{HIV}]}\right]^{1/2} \tag{3}$$

In eq 3 [HIV] is the total protease concentration in monomer units and ΔG the Gibbs energy of stabilization of the protease per mole of dimer. For the wild-type protease, we have previously measured (*20*) the different thermodynamic contributions that define the Gibbs energy of stabilization, including the enthalpy change (ΔH), entropy change (ΔS), heat capacity change (ΔC_p), and the pH dependence in terms of the protonation change (Δn_H) and the apparent pK_a in the unfolded and native states (p$K_{a,u}$, p$K_{a,n}$):

$$\Delta G_{wt} = \Delta H_{T_r} + \Delta C_p(T - T_r) - T[\Delta S_{T_r} + \Delta C_p \ln(T/T_r)] - RT\Delta n_H \ln[(1 + 10^{pK_{a,u}-pH})/(1 + 10^{pK_{a,n}-pH})] \tag{4a}$$

$$\Delta G_{wt} = -9000 + 3200(T - 298.15) - T[-76.0 + 3200 \ln(T/298.15)] - 4RT \ln[(1 + 10^{4.3-pH})/(1 + 10^{2.9-pH})] \tag{4b}$$

where the reference state is the native state at pH 5.5 and 25 °C. The effects of a mutation can be represented by an additional contribution to the Gibbs energy as follows:

$$\Delta G_{mut} = \Delta G_{wt} + \Delta\Delta G_{mut} \tag{5}$$

Figure 3B shows the dependence of the temperature dena-

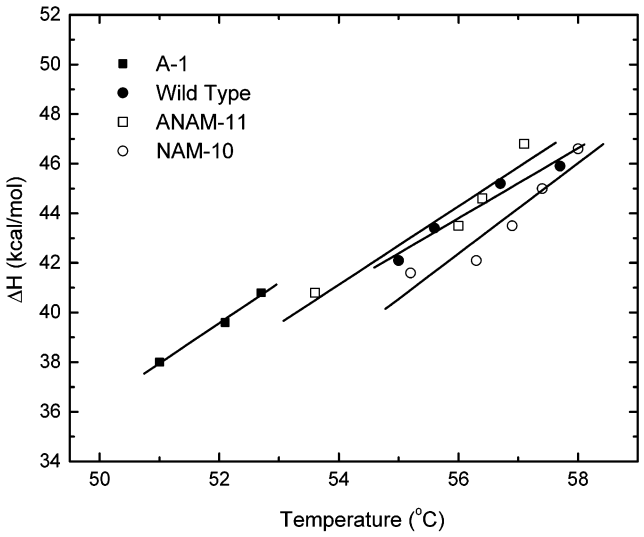

FIGURE 4: Dependence of the enthalpy change (ΔH) on the midpoint of temperature denaturation (T_m) for the wild-type and the mutant proteases, A-1, NAM-10, and ANAM-11. The enthalpy change was obtained from the area under the DSC curve at the corresponding protease concentration. The heat capacity changes (ΔC_p) obtained from the least-squares analysis (solid lines) for all of the proteases were within experimental error and average 3.2 ± 0.6 kcal K^{-1} (mol of dimer)$^{-1}$.

turation (T_m) on protease concentration. It is clear that the active site mutant protease, A-1, is significantly less stable than the wild type, whereas the non-active site mutant, NAM-10, is more stable than the wild type. ANAM-11 is not as stable as NAM-10 but still more stable than the wild type. The solid lines represent the expected concentration dependence of T_m calculated according to eqs 4 and 5. In this analysis, all of the parameters that define the stability of the wild-type protease (eq 4) were kept fixed, $\Delta\Delta G_{mut}$ being the only fitting parameter. The results of this analysis indicate that the active site mutation destabilizes the native structure of the protease by 1.2 kcal/mol while the non-active site mutations effectively compensate the destabilization effect as demonstrated by the observation that ANAM-11 is 0.15 kcal/mol more stable than the wild type. It must be noted that the effects of the different mutations are not additive since the non-active site mutations alone only stabilize the wild-type protease by 0.3 kcal/mol.

At equivalent temperatures the enthalpy changes were within ±4 kcal/mol of dimer for all proteases, which is within experimental error for calorimetric scans. Nevertheless, close examination of the enthalpy data (Figure 4) suggests that the enthalpy change for A-1 is systematically higher than that of the wild type whereas that of NAM-10 is lower. Since A-1 is less stable than NAM-10, this result indicates that the gain in enthalpy is compensated by a larger loss in entropic contributions to the Gibbs energy of stabilization. The opposite is true for NAM-10, in which the loss of enthalpic interactions is compensated by larger entropic gains. The heat capacity changes for all proteases are within experimental error and average 3.2 ± 0.6 kcal K^{-1} (mol of dimer)$^{-1}$. In all, the mutations influence the Gibbs energy of stabilization by small enthalpy and entropy variations.

Structural Analysis of Non-Active Site Mutations. Since inhibitor binding is coupled to a conformational change, any mutation that structurally stabilizes the native state will influence the binding affinity by a factor equal to the additional energy required to elicit the change. In the case of ANAM-11, the mutation-associated changes in the Gibbs energy of binding for all inhibitors are much larger (5−7 kcal/mol) than the change in the Gibbs energy of stabilization (0.15 kcal/mol), indicating that most of the resistance effect does not arise from a perturbation in the energetics of the conformational change. If this is not the case, an alternative scenario is that the accumulation of non-active site mutations disrupts the geometry of the binding cavity, making it difficult for a conformationally constrained inhibitor to bind with high affinity. In this respect, analysis of the structure of the HIV-1 protease (PDB file 1hhp) reveals that the side chains of four of the mutated residues in ANAM-11 are over 95% buried from the solvent (Met 36, Ala 71, Leu 90, and Ile 93 as shown in Figure 5A). Except for Met 36, which is located in the hinge region of the flaps, the mutations of the buried residues at the core of the protease (Ala 71, Leu 90, and Ile 93) involve an increase in the volume of the mutated side chains (Figure 5B). This volume increase forces a repacking of amino acids at the protease core immediately beneath the active site. This effect, coupled to the volume decrease at the hinges of the flaps, is likely to induce geometric distortions in the active site cavity and, consequently, a substantial loss in binding affinity of inhibitors with limited adaptability. A distortion in binding site geometry can be observed in the crystallographic structure of a mutant protease containing a mutation at residue 71 (PDB files 1odx and 1odw). This hypothesis is supported by additional data (not shown) obtained for a second-generation inhibitor (KNI-764) showing that ANAM-11 only lowers the binding affinity of this inhibitor by a factor of 50. Even though the panel of mutations in ANAM-11 was

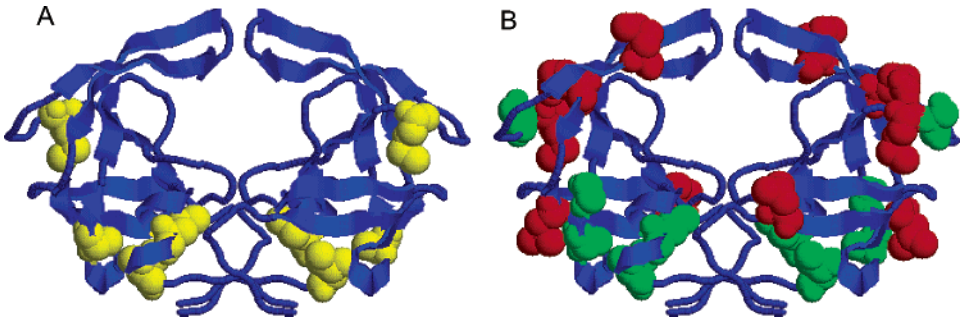

FIGURE 5: (A) Structure of the HIV-1 protease indicating in yellow the location of mutated residues with more than 95% of their side chains buried from the solvent (Met 36, Ala 71, Leu 90, and Ile 93). (B) Structure of the HIV-1 protease indicating, in green, the location of mutated residues that exhibit an increase in side chain volume and, in red, the location of mutated residues that exhibit a decrease in side chain volume.

not developed against KNI-764, we have shown previously (*6*, *32*) that this inhibitor has the capacity to adapt to several active site mutations. If the major mechanism of action of this set of non-active site mutations were a perturbation of the conformational energy barrier, the effect will be similar for all inhibitors that induce the same conformational change. This is not observed experimentally.

CONCLUSIONS

The experiments presented in this work clearly demonstrate that non-active site mutations are not limited to a compensatory role and that they may be mostly responsible for the observed loss in binding affinity of inhibitors. In fact, in the drug-resistant mutants studied in this work, the active site mutation is responsible for only a 10-fold or less loss in inhibitor affinity while the non-active site mutations lower inhibitor affinity by 3 orders of magnitude. Physiologically, drug-resistant mutations are usually classified in terms of their order of appearance in patients undergoing antiretroviral therapy. Primary mutations have been usually believed to be responsible for the loss of binding affinity of protease inhibitors. The studies presented here indicate that, even after the initial onset of resistance, the virus might still undergo additional mutations (including non-active site mutations) that lower the potency of inhibitors while still maintaining adequate catalytic efficiency.

REFERENCES

1. Hirsch, M. S., Brun-Vezinet, F., D'Aquila, R. T., Hammer, S. M., Johnson, V. A., Kuritzkes, D. R., Loveday, C., Mellors, J. W., Clotet, B., Conway, B., Demeter, L. M., Vella, S., Jacobsen, D. M., and Richman, D. D. (2000) *J. Am. Med. Assoc. 283*, 2417−2426.
2. Schock, H. B., Garsky, V. M., and Kuo, L. C. (1996) *J. Biol. Chem. 271*, 31957−31963.
3. Boden, D., and Markowitz, M. (1998) *Antimicrob. Agents Chemother. 42*, 2775−2783.
4. Nijhuis, M., Schuurman, R., de Jong, D., Erickson, J., Gustchina, E., Albert, J., Schipper, P., Gulnik, S., and Boucher, C. A. (1999) *AIDS 13*, 2349−2359.
5. Shafer, R. W. (2002) *Clin. Microbiol. Rev. 15*, 247−277.
6. Velazquez-Campoy, A., Kiso, Y., and Freire, E. (2001) *Arch. Biochem. Biophys. 390*, 169−175.
7. Freire, E. (2002) *Nat. Biotechnol. 20*, 15−16.
8. Ohtaka, H., Velazquez-Campoy, A., Xie, D., and Freire, E. (2002) *Protein Sci. 11*, 1908−1916.
9. Pazhanisamy, S., Partaledis, J. A., Rao, B. G., and Livingston, D. J. (1998) *Adv. Exp. Med. Biol. 436*, 75−83.
10. Markland, W., Rao, B. G., Parsons, J. D., Black, J., Zuchowski, L., Tisdale, M., and Tung, R. (2000) *J. Virol. 74*, 7636−7641.
11. Molla, A., Korneyeva, M., Gao, Q., Vasavanonda, S., Schipper, P. J., Mo, H. M., Markowitz, M., Chernyavskiy, T., Niu, P., Lyons, N., Hsu, A., Granneman, G. R., Ho, D. D., Boucher, C. A., Leonard, J. M., Norbeck, D. W., and Kempf, D. J. (1996) *Nat. Med. 2*, 760−766.
12. Markowitz, M., Conant, M., Hurley, A., Schluger, R., Duran, M., Peterkin, J., Chapman, S., Patick, A., Hendricks, A., Yuen, G. J., Hoskins, W., Clendeninn, N., and Ho, D. D. (1998) *J. Infect. Dis. 177*, 1533−1540.
13. Patick, A. K., Duran, M., Cao, Y., Shugarts, D., Keller, M. R., Mazabel, E., Knowles, M., Chapman, S., Kuritzkes, D. R., and Markowitz, M. (1998) *Antimicrob. Agents Chemother. 42*, 2637−2644.
14. Winters, M. A., Schapiro, J. M., Lawrence, J., and Merigan, T. C. (1998) *J. Virol. 72*, 5303−5306.
15. Olsen, D. B., Stahlhut, M. W., Rutkowski, C. A., Schock, H. B., vanOlden, A. L., and Kuo, L. C. (1999) *J. Biol. Chem. 274*, 23699−23701.
16. Perno, C. F., Cozzi-Lepri, A., Balotta, C., Bertoli, A., Violin, M., Monno, L., Zauli, T., Montroni, M., Ippolito, G., and d'Arminio-Monforte, A. (2002) *AIDS 16*, 619−624.
17. Cabana, M., Clotet, B., and Martinez, M. A. (1999) *J. Med. Virol. 59*, 480−490.
18. Hertogs, K., Bloor, S. D., Van den Eynde, C., Alcorn, T. M., Pauwels, R., Van Houtte, M., Staszewski, S., Miller, V., and Larder, B. A. (2000) *AIDS 14*, 1203−1210.
19. Condra, J. H., Petropoulos, C. J., Ziermann, R., Schleif, W. A., Shivaprakash, M., and Emini, E. A. (2000) *J. Infect. Dis. 182*, 758−765.
20. Todd, M. J., Semo, N., and Freire, E. (1998) *J. Mol. Biol. 283*, 475−488.
21. Velazquez-Campoy, A., Todd, M. J., Vega, S., and Freire, E. (2001) *Proc. Natl. Acad. Sci. U.S.A. 98*, 6062−6067.
22. Mildner, A. M., Rothrock, D. J., Leone, J. W., Bannow, C. A., Lull, J. M., Reardon, I. M., Sarcich, J. L., Howe, W. J., Tomich, C. S. C., Smith, C. W., Heinrikson, R. L., and Tomasselli, A. G. (1994) *Biochemistry 33*, 9405−9413.
23. Todd, M. J., Luque, I., Velazquez-Campoy, A., and Freire, E. (2000) *Biochemistry 39*, 11876−11883.
24. Velazquez-Campoy, A., Vega, S., and Freire, E. (2002) *Biochemistry 41*, 8613−8619.
25. Benson, D. A., Boguski, M. S., Lipman, D. J., Ostell, J., and Ouellette, B. F. (1998) *Nucleic Acids Res. 26*, 1−7.
26. Szeltner, Z., and Polgar, L. (1996) *J. Biol. Chem. 271*, 5458−5463.
27. Ridky, T. W., Kikonyogo, A., Leis, J., Gulnik, S., Copeland, T., Erickson, J., Wlodawer, A., Kurinov, I., Harrison, R. W., and Weber, I. T. (1998) *Biochemistry 37*, 13835−13845.
28. Klabe, R. M., Bacheler, L. T., Ala, P. J., Erickson-Viitanen, S., and Meek, J. L. (1998) *Biochemistry 37*, 8735−8742.
29. Sigurskjold, B. W. (2000) *Anal. Biochem 277*, 260−266.
30. Thompson, K. S., Vinson, C. R., and Freire, E. (1993) *Biochemistry 32*, 5491−5496.
31. Johnson, C. R., Angeletti, M., Pucciarelli, S., and Freire, E. (1996) *Biophys. Chem. 59*, 107−117.
32. Velazquez-Campoy, A., and Freire, E. (2001) *J. Cell. Biochem., Suppl. 37*, 82−88.

BI027019U